Journal of Human Evolution 62 (2012) 104–115

Contents lists available at SciVerse ScienceDirect

Journal of Human Evolution

journal homepage: www.elsevier.com/locate/jhevol

A chronological framework for a long and persistent archaeological record: Melka Kunture, Ethiopia

Leah E. Morgan [a,*,1], Paul R. Renne [a,b], Guy Kieffer [c], Marcello Piperno [d], Rosalia Gallotti [e], Jean-Paul Raynal [e,f]

[a] Department of Earth & Planetary Science, University of California, Berkeley, CA 94720, USA
[b] Berkeley Geochronology Center, 2455 Ridge Rd., Berkeley, CA, USA
[c] Italian Archaeological Mission at Melka Kunture and Balchit, 22 rue Paul Gaubin, 63450 Le Crest, France
[d] Dipartimento di Scienze dell'Antichità, Sapienza Università di Roma, Via Palestro 63, 00185 Rome, Italy
[e] Univ. Bordeaux 1, PACEA, UMR 5199, F-33400 Talence, France
[f] Department of Human Evolution, Max Planck Institute for Evolutionary Anthropology, Deutscher Platz 6, 04103 Leipzig, Germany

A R T I C L E I N F O

Article history:
Received 18 July 2011
Accepted 13 October 2011

Keywords:
$^{40}Ar/^{39}Ar$ geochronology
Oldowan
Acheulean
Obsidian
Upper Awash
Ethiopia

A B S T R A C T

New $^{40}Ar/^{39}Ar$ geochronological data for several volcanic ash horizons from Melka Kunture, Ethiopia, allow for significantly more precise age constraints to be placed upon the lithostratigraphy, archaeology and paleontology from this long record. Ashes from the Melka Kunture Formation at Gombore yielded the most reliable age constraints, from 1.393 ± 0.162 Ma[2] (millions of years ago) near the base of the section to 0.709 ± 0.013 Ma near the top. Dating the Garba section proved more problematic, but the base of the section, which contains numerous Oldowan obsidian artifacts, may be >1.719 ± 0.199 Ma, while the top is securely dated to 0.869 ± 0.020 Ma. The large ignimbrite from the Kella Formation at Kella and Melka Garba is dated to 1.262 ± 0.034 Ma and pre-dates Acheulean artifacts in the area. The Gombore II site, which has yielded two *Homo* skull fragments, 'twisted bifaces,' and a preserved butchery site, is now constrained between 0.875 ± 0.010 Ma and 0.709 ± 0.013 Ma. Additional ashes from these and other sites further constrain the timing of deposition throughout the section.

Integration with previously published magnetostratigraphy has allowed for the first time a relatively complete, reliable timeline for the deposition of sediments, environmental changes, archaeology, and paleontology at Melka Kunture.

Introduction

History and importance

The site of Melka Kunture includes several localities located on the banks of the Awash River and on the shoulder of the Ethiopian Rift (Figures 1 and 2). The archaeological potential of the area was first recognized by hydrologist Gerard Dekker in 1963 (Chavaillon and Piperno, 2004b) and was first extensively surveyed by Gerard Bailloud in 1963 and 1964 (Bailloud, 1965). Excavations were led by Jean Chavaillon from 1965 to 1995. Since 1999, they have been led by Marcello Piperno (Chavaillon and Piperno, 2004b). Archaeology found at these sites includes artifacts from every major period of the African archaeological record from the Oldowan to the Late Stone Age (Chavaillon and Berthelet, 2004).

Frequently, evidence bearing on human evolution varies both spatially and temporally. Evidence from a particular time period is collected from sites that are hundreds to thousands of kilometers apart and it is relatively rare to find multiple time periods represented within a small area. At Melka Kunture, however, the collection of localities in such close proximity and covering such a wide variety of archaeological technologies (and presumably time) can potentially add a great deal to our understanding of the biological and behavioral evolution of human ancestors over time in this one region. By better constraining the chronology of the localities at Melka Kunture using modern geochronological techniques, the formal lithostratigraphic units (Raynal et al., 2004),

* Corresponding author.
E-mail addresses: leah.morgan@glasgow.ac.uk (L.E. Morgan), prenne@bgc.org (P.R. Renne), g.m.kieffer@wanadoo.fr (G. Kieffer), m.piperno@tin.it (M. Piperno), rosalia.gallotti@pacea.u-bordeaux1.fr (R. Gallotti), jp.raynal@pacea.u-bordeaux1.fr (J.-P. Raynal).
[1] Present address: Scottish Universities Environmental Research Centre, Scottish Enterprise Technology Park, Rankine Avenue, East Kilbride, G75 0QF, United Kingdom.
[2] Uncertainties are provided at 1σ, here and throughout.

0047-2484/$ – see front matter © 2011 Elsevier Ltd. All rights reserved.
doi:10.1016/j.jhevol.2011.10.007

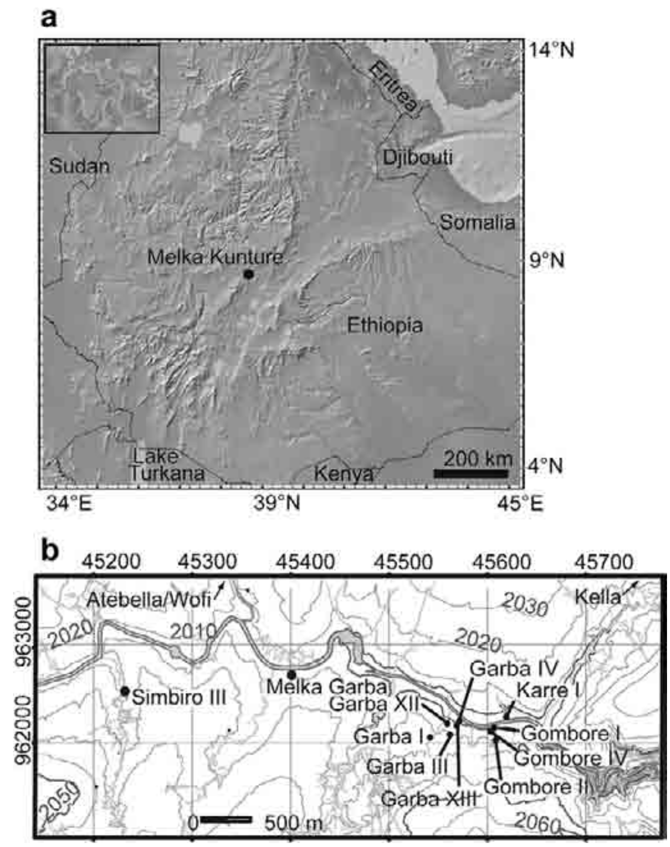

Figure 1. a. Map of Ethiopia and surrounding countries. The location of Melka Kunture is marked on the shoulder of the Main Ethiopian Rift. b. Map of the Melka Kunture area. Modified from map by Riccardo Salvini and Maria Cristina Salvi and created on a U.T.M. Zone 37 Grid using a transverse Mercator projection, Clarke 1880 spheroid, and the Adindan (Arc) datum.

archaeology, and paleontology found there can be placed into the larger temporal and spatial framework in the process of being established for eastern Africa.

Archaeology

Archaeological details for many sites at Melka Kunture have been published previously by Chavaillon and Chavaillon (1976), Chavaillon and Berthelet (2004), and references therein. Oldowan sites include Gombore I, Garba IV, Karre I, and Kella III (Chavaillon and Chavaillon, 1976). Gombore Iγ is considered a 'Developed Oldowan' site. Early Acheulean localities include Garba XIII (only excavated since 2007 and still unpublished), Garba XII and Simbiro III. Assemblages from Gombore II and Garba I are considered to be Middle and Late Acheulean, respectively. Garba III is thought to contain an Acheulean-Middle Stone Age transition and has been compared with the assemblage from Herto in the Middle Awash of Ethiopia (Clark et al., 2003). Artifacts from Kella I, Wofi III, and Wofi IV are thought to represent the Late Stone Age.

Among the most conspicuous features of the archaeology at Melka Kunture is the frequent use of obsidian as a raw material, including the Oldowan sites of Garba IV and Gombore I (Piperno et al., 2009). Elsewhere in eastern Africa, obsidian was, for the most part, exploited as a raw material for tool making only from the Middle Stone Age onwards (Leakey, 1931; Merrick and Brown, 1984), although it is found at several Acheulean sites. Acheulean obsidian occurrences include intensive use (i.e., >100 artifacts) at Kariandusi (Kenya) at ~0.7–1.0 Ma (millions of years ago) (Gowlett and Crompton, 1994), and less intensive use (i.e., <10 artifacts) at Kilombe (Kenya) at >0.7 Ma (Crompton and Gowlett, 1993; Gowlett, 1993), Olorgesaile (Kenya) at 0.992 ± 0.039–0.493 ± 0.001 Ma (Isaac, 1977; Deino and Potts, 1990), Gadeb (Ethiopia) (>0.7 Ma, and possibly >1.48 Ma), based on unpublished K–Ar dating of an overlying alluvial unit (Clark, 1979; Williams et al., 1979), and the Dawaitoli Formation in the eastern Middle Awash region of Ethiopia at ~0.64 Ma (Clark and Schick, 2000). Melka Kunture, therefore, is the location of the only known use of obsidian for the manufacture of Oldowan tools, and one of only a few for Acheulean tools (Piperno et al., 2009). This obsidian is sourced from Balchit, an obsidian dome-flow ~7 km to the north (Poupeau et al., 2004; Negash et al., 2006), and was likely available from there to the Awash river along drainage networks. Geochronological data presented here helps constrain the age of these early obsidian artifacts, as well as many younger artifacts previously lacking age constraints.

Also of particular note are the 'twisted bifaces' found at Gombore II (Chavaillon, 1979a; Gallotti et al., 2010), which are the only known excavated in Africa. Similar artifacts have otherwise only been found as part of a surface collection near Lake Langano (Chavaillon, 1979b). They are also present at several localities in the British Lower Paleolithic, wherein it has been suggested that this type of bifaced tool was used for animal butchery, particularly scraping, rather than cutting (Walter, 1996), although others (White, 1998; Gallotti et al., 2010) find that more detailed use-wear studies are necessary before a specific function can be identified conclusively. Although a specific function or importance cannot yet be determined for the twisted bifaces found at Melka Kunture, their scarcity elsewhere in eastern Africa is striking compared with their abundance at Gombore II.

Hominids

The hominid fossils found at Melka Kunture have been described previously (Chavaillon et al., 1974; Chavaillon and Coppens, 1975; Chavaillon et al., 1977; Chavaillon and Coppens, 1986; Chavaillon et al., 1987; Condemi, 2004; Coppens, 2004; Zilberman et al., 2004a, 2004b) and include four apparent *Homo erectus* (sensu lato) specimens and one probable archaic *Homo sapiens*. The apparent *H. erectus* humerus from Gombore I is considered by some to be too robust to be a *Homo habilis*, although the latter is much more commonly associated with the Oldowan-type archaeology from this site (*H. erectus* is commonly found with Acheulean archaeology). Similarly, the partial mandible of an apparent *H. erectus* infant has been found at Garba IV, also associated with Oldowan archaeology. Yet two other specimens of *H. erectus* (skull fragments) have been found at the Gombore II Locality 1, where they are associated with Acheulean archeology. Three *H. sapiens* cranial fragments have been found at Garba III, where they are associated with Late Acheulean artifacts.

Vertebrate paleontology (excluding hominids), paleoenvironments, and lithostratigraphy

The vertebrate paleontology at the Melka Kunture sites is dominated by the order Cetartiodactyla (Montgelard et al., 1997) and includes bovids, giraffids, hippopotamids, and suids, as well as primates. With few exceptions, the fossil material is postcranial or dental. Faunal information has also been previously published (Geraads, 1979; Chavaillon and Berthelet, 2004; Geraads et al., 2004). Nearly all of the localities include *Hippopotamus* sp. and other artiodactyls that are commonly found in or near aqueous environments, along with species thought to be grazers that are more commonly found in dry, open savannah environments (Geraads, 1979; Geraads et al., 2004). Stable isotope data, in

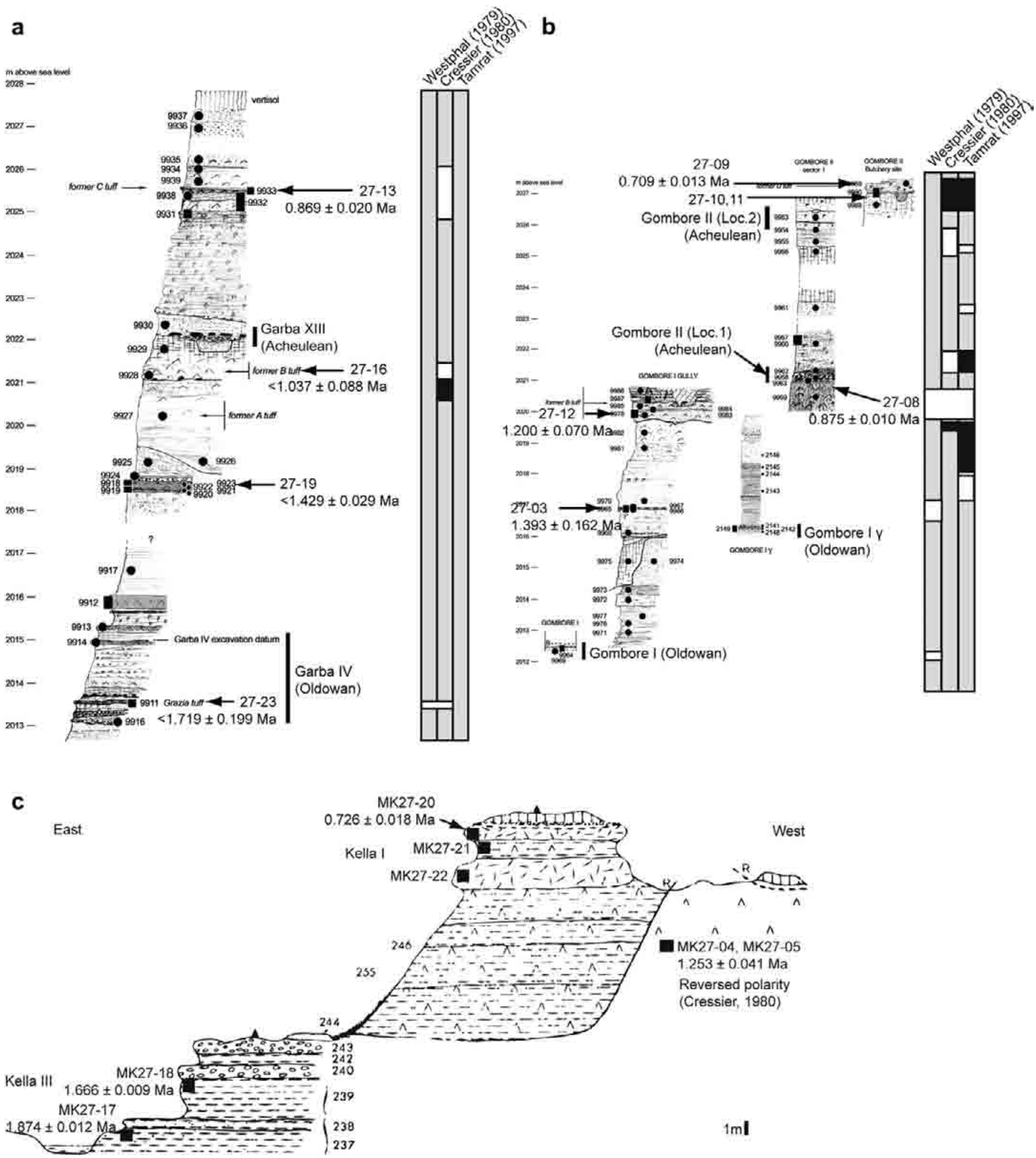

Figure 2. a. Stratigraphic section of the Garba area, Melka Kunture. Modified from Raynal et al. (2004). b. Stratigraphic section of the Gombore area, Melka Kunture. Modified from Raynal et al. (2004). c. Cross section of the Kella area, Melka Kunture. Modified from Taieb (1974). For a, b, c: K–Ar ages from Schmitt et al. (1977), new $^{40}Ar/^{39}Ar$ ages from this study; magnetostratigraphy from Cressier (1980), Westphal et al. (1979) and Tamrat (1997).

particular the $\delta^{13}C$ values of mostly $\sim 0‰$ (PDB) on bovid and equid fossil tooth enamel, support the presence of open C_4 grasslands (Bocherens et al., 1996).

The architecture and facies of lithostratigraphic units, particularly the channeling processes and sediment facies (coarse gravels, sands, and clays; largely volcanic), are consistent with fluvial and associated floodplain depositional environments of the paleo-Awash river and its tributaries (Raynal et al., 2004). Recurrent tectonic events, as well as volcanic inputs that are evidenced by several volcanic ashes in primary and sub-primary positions, have frequently interfered with the climatically-driven sedimentary processes (Raynal and Kieffer, 2004).

The lithostratigraphic, faunal, and isotopic evidence suggests that these floodplains and other areas surrounding the river were likely dry, open savannahs. The presence of evidence of hominid activity is thus not surprising, as hominid fossils and artifacts are often found at the interface between land and freshwater (Hay, 1976).

Previous geochronology: K–Ar and magnetostratigraphy

Previous geochronology at Melka Kunture included K–Ar and paleomagnetic analyses. K–Ar data were never formally published but are often attributed to an abstract by Schmitt et al. (1977). The abstract cited does not actually contain K–Ar ages (which were likely reported only orally at the conference), but the apparent results are cited in the monograph edited by Chavaillon and Piperno (2004a). Many of these analyses were performed on glass shards, which are known to yield spurious apparent ages due to post-depositional potassium and/or argon mobility within the glass (Cerling et al., 1985; Morgan et al., 2009). Additionally, the stratigraphic context of the analyzed samples was not well described, further undermining the utility of these previously undocumented K–Ar results. The best estimates for the locations of these samples are shown in Figure 2(a, b, c).

Paleomagnetic analyses were published by Westphal et al. (1979), Cressier (1980), and Tamrat (1997), however correlations between their stratigraphic sections (and associated magnetic polarity stratigraphy) and the more recent sections published by Raynal et al. (2004) are not always clear. When a correlation can be made with confidence, magnetostratigraphic results are shown Figure 2(a, b, c).

The chronostratigraphic significance of paleomagnetic data is difficult to interpret without reliable absolute ages to determine which magnetic reversals are recorded in the sediments, i.e., to facilitate unambiguous correlation of magnetostratigraphy with the geomagnetic polarity time scale (Gradstein et al., 2004). New $^{40}Ar/^{39}Ar$ geochronological data presented here, when combined with previous paleomagnetic work, thus help to constrain the ages of the artifacts found at several Melka Kunture localities.

Methods

Sample collection

Tephra samples were collected at Melka Kunture in October 2007 and November 2008, in close collaboration with geologists and archaeologists working on the sites. Care was taken to avoid contamination in the form of root cast infillings and modern roots when possible, although in some cases this was inevitable. Sample locations were recorded with a handheld GPS unit using the WGS 84 reference coordinate system (Table 1). Care was also taken to accurately place and name samples according to the previously published formal lithostratigraphy (Raynal et al., 2004).

Electron microprobe geochemistry

The geochemistry of glass shards from volcanic ashes was measured with a Cameca XS-51 electron microprobe in the Department of Earth and Planetary Science at the University of California, Berkeley. A 10 μm rastered beam at 15 nA and 15 kV was used to limit volatilization of mobile elements in glass. Multiple points ($n = 2–5$) were measured on each shard. Multiple shards ($n = 5–15$) were measured from each sample. Obvious outliers, including measurements inadvertently made on mineral grains (feldspars, pyroxenes, etc.) or void-filling epoxy, were omitted from further consideration.

$^{40}Ar/^{39}Ar$ geochronology

Volcanic ash samples were prepared and measured as in Morgan and Renne (2008). Samples were co-irradiated with the Alder Creek sanidine (ACs) (Nomade et al., 2005) standard using the standard and decay constant calibration published by Renne et al. (2010). Values used for nucleogenic production ratios are as in Renne et al. (2005). The atmospheric $^{40}Ar/^{36}Ar$ ratio of Steiger and Jäger (1977) was used. More recent determinations of atmospheric $^{40}Ar/^{36}Ar$ give $\sim$1% higher values (Lee et al., 2006; Valkiers et al., 2010), but as shown by Renne et al. (2009) this has negligible impact on age calculations because the same value was used to determine mass discrimination and the air correction. $^{40}Ar/^{39}Ar$ geochronology was performed at the Berkeley Geochronology Center as in Morgan and Renne (2008). Background values were constrained by measuring blanks every $\sim$ three analyses. Mass discrimination was monitored by measuring air pipette aliquots every $\sim$10–15 analyses. Full data are provided in Supplementary Table 1. Single crystal total fusion (SCTF) was performed on all samples with the exception of MK27-13, which has sufficiently small crystals that multigrain total fusion analyses were necessary. Finally, MK27-09 and −20 were subjected to multigrain step-heating experiments in addition to the SCTF.

Results

Electron microprobe geochemistry and potential correlations

Full data are provided in Supplementary Table 2, including individual shard averages and values for the standard error of the mean (shown in italics). The one exception to this is sample MK27-04, for which it was not possible to visually relocate microprobe points after analysis. Thus, each analysis for this sample is treated individually because the correspondence between analyses and individual shards is ambiguous.

Geochemical data were visualized and analyzed using JMP® version 7.0 (SAS Institute Inc., 2007). A plot of the first two principal components based on correlations of all measured oxides (except relatively volatile oxides Na_2O and K_2O) is shown in Figure 3. Each point represents a single measured shard. Each individual color/shape combination represents a sample. Visual inspection allows for identification of potential correlative units, which are discussed below.

Group A (samples MK27-01, 04, 05, 16) Since samples MK27-04 and MK27-05 were taken from the same outcrop of a non-welded ignimbrite at Kella, their correlation is reliable. Sample MK27-01 was taken from another outcrop of ignimbrite at Melka Garba that was previously believed to be the same lithostratigraphic unit (Raynal and Kieffer, 2004) that forms the Kella Formation (Raynal et al., 2004). The similar geochemistry of these three samples seems to confirm that correlation.

The geochemistry of MK27-16, from a tuff underlying Garba XIII in the Garba gully, overlaps with the others in this group in most oxides, which the exception of Al_2O_3. Although there is only a slight difference, when combined with the mineralogical differences between this tuff and the others, this correlation is tenuous at best. As shown below, MK27-01 and MK27-05 have very similar ages. MK27-16 differs more but is also indistinguishable in age (at the 2σ level) from these two units. An age for MK27-04 was not determined. See Table 2 for details.

Group B (Samples MK27-09, 11, 12, 13, 20) Samples MK27-09 and MK27-20 show very slight differences in SiO_2 concentration, but

Table 1
Sample descriptions, locality name, formation, and unit (Raynal et al., 2004), and GPS coordinates for tephra sampled at Melka Kunture.

Sample	Description	Locality	Formation	Unit	Latitude	Longitude
27–01	Pumice clasts from ignimbrite	Melka Garba	Kella F.	N/A	N/A	N/A
27–02	Lithics and pumices from degassing pipe within ignimbrite	Melka Garba	Kella F.	N/A	N/A	N/A
27–03	Light gray-brown, fine-grained volcanic ash	Gombore I	Melka Kunture F.	9965–9967	N08°42.333′	E038°36.094′
27–04	Pumice clasts from ignimbrite	Kella	Kella F.	N/A	N08°42.881′	E038°36.602′
27–05	Base surge of ignimbrite	Kella	Kella F.	N/A	N08°42.881′	E038°36.602′
27–06	Volcanic ash ~20 cm thick white fine w/xtals	Wofi	–	N/A	N08°43.311′	E038°34.568′
27–07	Dark gray indurated volcanic ash	Garba XII	Melka Kunture F.	N/A	N08°42.371′	E038°35.866′
27–08	White, fine-grained volcanic ash with xtals	Gombore II	Melka Kunture F.	9959	N08°42.314′	E038°36.098′
27–09	Crystal- and pumice-rich tuff	Gombore II	Melka Kunture F.	9989	N08°42.284′	E038°36.098′
27–10	Crystal-rich bentonite	Gombore II	Melka Kunture F.	9988	N08°42.284′	E038°36.098′
27–11	Crystal-rich bentonite	Gombore II	Melka Kunture F.	9988	N08°42.284′	E038°36.098′
27–12	Ash flow tuff, sampled just above surge deposit	Gombore I	Melka Kunture F.	9978	N08°42.339′	E038°36.092′
27–13	Very fine-grained, light gray-blue volcanic ash (former C tuff)	Garba Gully	Melka Kunture F.	9933	N08°42.322′	E038°35.892′
27–14	Very fine-grained, light gray-blue volcanic ash	Simbiro	–	N/A	N08°42.506′	E038°33.989′
27–15	Tuffaceous sandstone	Simbiro	–	N/A	N08°42.502′	E038°33.988′
27–16	Gray, medium-grained volcanic ash (former B tuff)	Garba Gully	Melka Kunture F.	9928	N08°42.343′	E038°35.904′
27–17	White, medium-grained volcanic ash	Kella	Melka Kunture F.	N/A	N08°42.929′	E038°36.739′
27–18	White, fine-grained volcanic ash	Kella III	Melka Kunture F.	N/A	N08°42.901′	E038°36.718′
27–19	Light gray-brown, fine-grained volcanic ash	Garba Gully	Melka Kunture F.	9918–9923	N08°42.354′	E038°35.906′
27–20	Crystal- and pumice-rich tuff	Kella I	Melka Kunture F.	N/A	N08°42.920′	E038°36.677′
27–21	Crystal-rich bentonite	Kella I	Melka Kunture F.	N/A	N08°42.920′	E038°36.677′
27–22	Crystal- and pumice-rich tuff	Kella I	Melka Kunture F.	N/A	N08°42.920′	E038°36.677′
27–23	Very fine-grained, gray volcanic ash	Garba IV	Melka Kunture F.	9911	N08°42.384′	E038°35.920′
2005–10	Crystal- and pumice-rich tuff	Simbiro	–	N/A	N/A	N/A

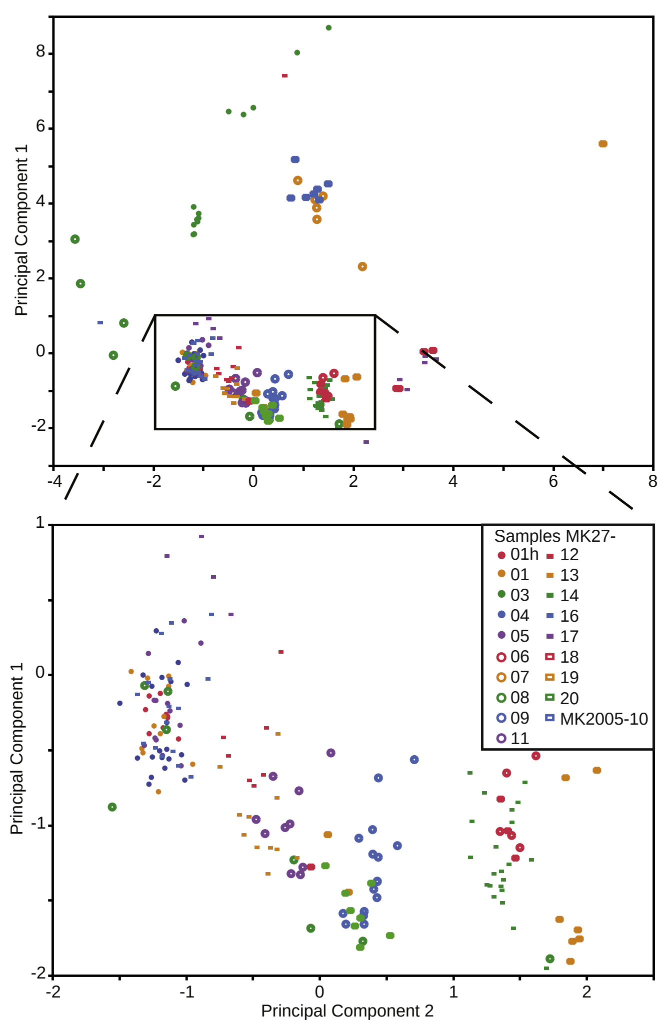

Figure 3. Principal component analysis of electron microprobe geochemical data. The mean value for each shard is represented by a data point. The first two principal components, which are shown here, represent 75.2% of the variation in the data.

other oxides are overlap considerably. When this is considered along with their similar mineralogies and their respective locations near the top of the Melka Kunture Formation at the Gombore II and Kella I sections, this correlation is highly probable. $^{40}Ar/^{39}Ar$ ages for these two tuffs (provided below) are indistinguishable (Table 2).

Sample MK27-12 shows slight, but clear distinctions from all other sampled units. The $^{40}Ar/^{39}Ar$ age for this unit is significantly older than those for the other geochemically similar units (Table 2). The possibility remains that this unit formed from an eruptive sequence that also formed the non-welded ignimbrite (MK27-01, MK27-05), as their ages are indistinguishable (Table 2) and their geochemistry is distinct but reasonably similar.

Considering the stratigraphic proximity, and geochemical and mineralogical similarities between MK27-09 and MK27-11, it is highly likely that they are derived from the same volcanic system. MK27-12, MK27-13, and MK27-20 may also derive from this same system, although differences in age suggest that they were erupted over a significant time period. MK27-12 may also contain antecrysts.

Group C (Samples MK27-06, 14) Although in Principal Component space these two samples overlap considerably (Figure 3), several oxides show discrepancies when considered individually (Supplementary Table 2). No correlation is made here.

Group D (samples MK27-07, MK2005-10) These two samples show considerable overlap in both Principal Component space and also in all measured oxides, thus a correlation is likely. $^{40}Ar/^{39}Ar$ geochronological data for MK27-07 are imprecise, but consistent with this correlation.

$^{40}Ar/^{39}Ar$ geochronology

The tephras intercalated in Melka Kunture strata vary from ignimbritic deposits that are many meters thick to fine distal ashes of only a few centimeters thickness. Some are apparently free of xenocrystic contamination, while others contain significant contamination. This may have occurred during eruption or by post-depositional reworking. Feldspar compositions include mostly anorthoclase and sanidine, although plagioclase is found in some samples. Specifics for each sample, as determined by isotopic ratios

Table 2
Plateau and isochron ages for each dated sample from Melka Kunture. The most reliable age for each unit (based on quality of MSWD and P; see text for details) is shown in bold.

Sample	Weighted mean age				Inverse isochron						Feldspar(s) analyzed[e]
	Age	Error	MSWD	P	Age	Error	$^{40}Ar/^{36}Ar$	$\pm^{40}Ar/^{36}Ar$	MSWD	P	
27–01	1.260	0.110	1.07	0.38	**1.281**	**0.061**	293	3	1.10	0.33	Sanidine and/or Anorthoclase
27–03	1.400	0.120	0.18	0.97	**1.393**	**0.162**	300	400	0.22	0.93	Anorthoclase
27–05	1.260	0.030	1.61	0.03	**1.253**	**0.041**	320	20	1.60	0.03	Anorthoclase
27–06	0.870	0.060	0.06	1.00	**0.890**	**0.081**	240	200	0.07	0.99	Sanidine and/or Anorthoclase
27–07[a]	**0.772**	**0.091**									Anorthoclase
27–08	**0.875**	**0.010**	1.36	0.18	0.879	0.015	289	10	1.50	0.13	Sanidine and/or Anorthoclase
27–09	**0.709**	**0.013**	0.64	0.93	0.697	0.020	320	20	0.61	0.94	Sanidine and/or Anorthoclase
27–09[b]	0.742	0.022	0.72	0.49	0.740	0.009	296	13	1.70	0.04	Sanidine and/or Anorthoclase
27–11c	0.719	0.013	2.56	0.00	0.516	0.041	670	160	1.50	0.03	Sanidine and/or Anorthoclase
27–12	**1.200**	**0.070**	0.36	0.96	1.100	0.202	600	600	0.29	0.98	Sanidine and/or Anorthoclase (plagioclase)
27–13	0.870	0.019	0.73	0.57	**0.869**	**0.020**	295	3	0.97	0.41	Sanidine and/or Anorthoclase (plagioclase)
27–16[a]	**1.037**	**0.088**									Sanidine and/or Anorthoclase (plagioclase)
27–17	**1.874**	**0.012**	3.41	0.00	1.851	0.040	340	60	3.70	0.00	Anorthoclase (plagioclase)
27–18	**1.666**	**0.009**	0.59	0.92	1.637	0.020	320	16	0.51	0.95	Sanidine and/or Anorthoclase
27–19[a]	**1.429**	**0.029**									Sanidine and/or Anorthoclase
27–20	0.746	0.009	1.81	0.01	**0.726**	**0.018**	330	20	1.70	0.03	Sanidine and/or Anorthoclase
27–20[b]	0.797	0.012	0.06	0.98	0.795	0.017	310	140	0.09	0.92	Sanidine and/or Anorthoclase
27–23[d]	1.570	0.150	0.60	0.66	**1.719**	**0.199**	220	110	0.73	0.54	Sanidine and/or Anorthoclase
2005–10	0.883	0.008	0.64	0.93	**0.878**	**0.014**	307	19	0.66	0.91	Anorthoclase

[a] From youngest single valid crystal. Only valid as minimum age.
[b] Weighted mean of plateau ages from step-heating data.
[c] No age is selected here because isochron and weighted mean ages are not in agreement.
[d] From youngest 5 crystals. See text for explanation.
[e] Secondary minerals shown in parentheses.

and by viewing grain mounts of feldspars under oils on a petrographic microscope, are noted in Table 2.

The results presented below are summarized in Table 2. Full argon isotopic data and data required for isochron analysis are presented in Supplementary Table 1. Data from stratigraphically and paleoanthropologically significant samples are shown in relative probability diagrams and isochrons in Figures 4–6. Analyses with ^{40}Ar signals less than three times the applied ^{40}Ar blank correction are omitted from age calculations and shown near the end of Supplementary Table 1. Many analyses yielded small and frequently apparently negative ^{37}Ar (produced from Ca in the reactor) signals, resulting from low Ca abundances and long delays (up to 11 months) between irradiation and analysis coupled with the short half-life of ^{37}Ar (Renne and Norman, 2001). Apparently negative ^{37}Ar values imply an overcorrection for the blank, but all are within 2σ of zero and are thus retained in order to avoid imposing statistical bias. Steps with <3% of total ^{39}Ar released in incremental-heating experiments are not included in the calculation of isochron ages, mainly because relatively small ion beams are measured less precisely and highly imprecise data can exert undue influence on some statistical parameters, such as the Mean Squared Weighted Deviates (MSWD). Adoption of the isochron age as the most reliable age is made when isochron MSWD is <2.5 and >0.5 and isochron probability of fit P is <0.85 and >0.15. When these conditions are not met, the age with better MSWD (closer to 1) and P (closer to 0.5) is accepted as the most reliable age. All values are provided in Table 2. The age and error with better associated MSWD and P are shown there in bold. For all samples except one, weighted mean and isochron ages are indistinguishable at the 1σ level. No age is assigned where this is not the case (MK27-11). Problematic or otherwise noteworthy samples are discussed below. Ages provided below include both model ages (i.e., weighted mean and plateau ages), which require assuming an atmospheric $^{40}Ar/^{36}Ar$ value, and inverse isochron ages, which do not require this assumption.

MK27-01, MK27-05 The weighted mean age of the isochron ages for these two samples is 1.262 ± 0.034 Ma.

MK27-06 The inverse isochron here is poorly constrained. The MSWD and P are beyond the acceptable range (defined above) but are slightly better than those for the weighted mean age. Thus, the inverse isochron age is adopted as the more reliable age for this unit.

MK27-07 This sample has no clearly-defined juvenile population. However, since the tuff overlies the archaeology at Garba XII, the youngest crystal can serve as a valid minimum age here.

MK27-09 Due to the presence of a single juvenile population with no apparent xenocrysts, as shown in Figure 5(A, B), multigrain separates from MK27-09 were incrementally heated. Three of the four step-heating experiments yielded plateau ages (Figure 5C). The weighted mean of these is 0.742 ± 0.022 Ma. An isochron age, including steps from the same three aliquots that have >3% of the total ^{39}Ar released, yield an age of 0.740 ± 0.009 Ma (Figure 5D). The slightly higher (in one case distinguishable at 1σ) ages obtained by the multigrain step-heating experiments could be caused by xenocrystic contamination not apparent in the single crystal data. Considering that the age of the unit is a constraint on underlying archaeology and paleontology, the slightly younger, and less well-constrained, weighted mean age of single crystals (0.709 ± 0.013 Ma) is considered a more reliable and valid age for this unit.

MK27-11 The weighted mean model age for this unit differs significantly from the isochron age, although the initial $^{40}Ar/^{36}Ar$ value is very imprecise (670 ± 160). Since the sample was taken from a tuff directly underlying the tuff from which sample MK27-09 was taken, and since MK27-09 yields a much more reliable age, we do not interpret an age for this unit.

MK27-12 When analyses yielding less than three times the applied background correction are omitted, a juvenile population becomes apparent (Figure 4). An inverse isochron of the juvenile population of crystals yields little spread but similar MSWD and P to the weighted mean age (Figure 4D). The weighted mean age is selected here as more reliable due to superior MSWD and P, as well as the lack of sufficient spread on the isochron.

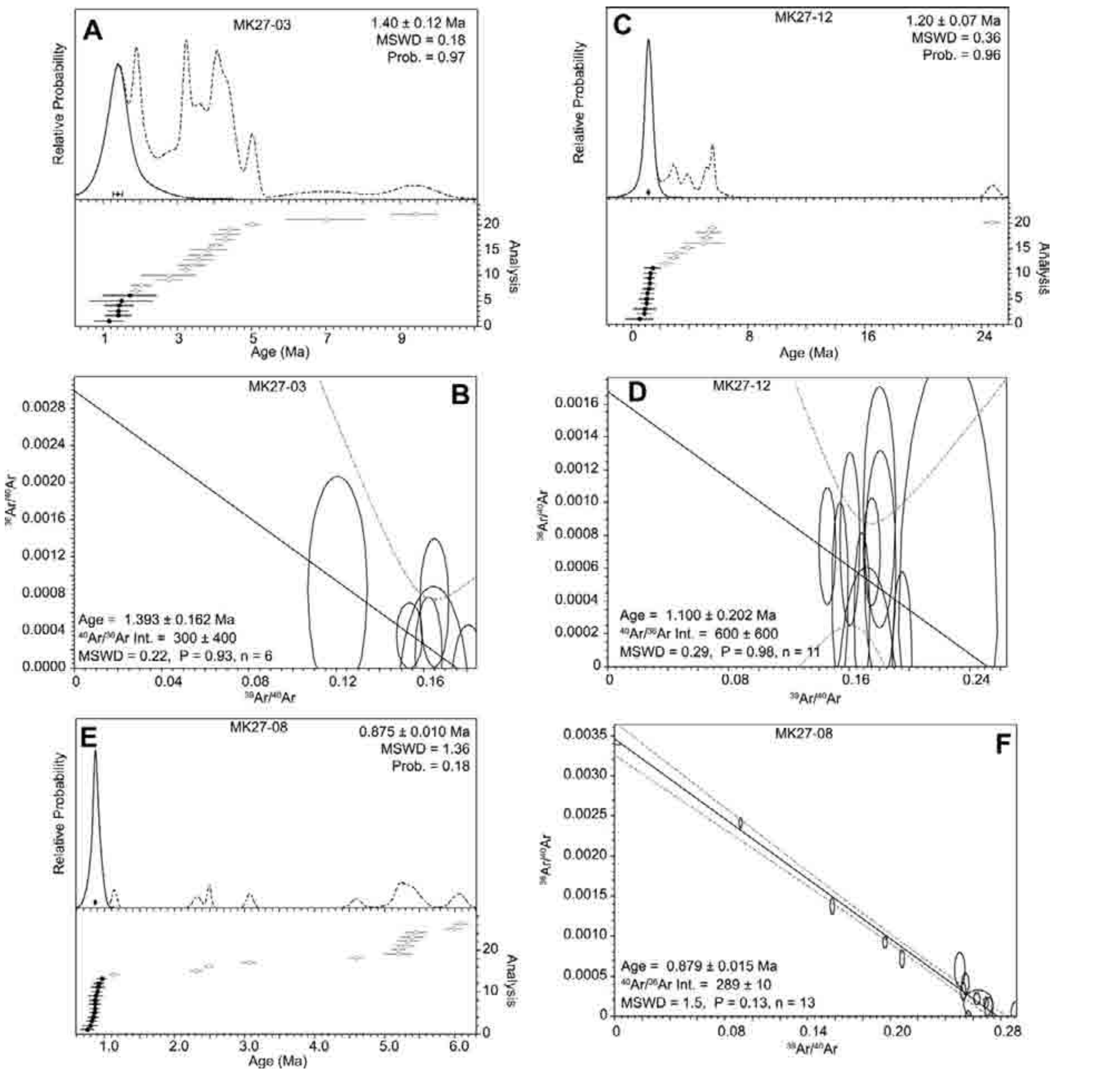

Figure 4. Age probability diagrams and inverse isochrons for single crystal total fusion data from (A, B)MK27-03, (C, D)MK27-12, and (E, F)MK27-08. Apparent xenocrysts are shown in gray in age probability diagrams and are not shown on isochrones. These are omitted from all age calculations. Only analyses with sufficient ^{40}Ar (more than three times blank) are shown here. Isochrons include only analyses from apparent juvenile populations.

MK27-13 Individual grains separated from this fine-grained distal ash were too small (~180–200 μm) to yield sufficient gas for analysis, so multiple grains ($n \approx 50$) were analyzed in each aliquot. One analysis was omitted for poor ion beam evolution as a function of time, and another is significantly older than the remaining aliquots (Figure 5G). The weighted mean and inverse isochron (Figure 5H) of the potentially juvenile population yield nearly identical ages of 0.870 ± 0.019 and 0.869 ± 0.020 Ma. The possibility of xenocrystic contamination is very high here, especially considering the number of crystals analyzed with no previous single crystal work, but this age is remarkably reproducible, suggesting the presence of little to no contamination.

MK27-16 No obvious juvenile population exists here, although there is a significant xenocrystic population at ~5 Ma. The ages of remaining crystals are scattered. The youngest crystal has a ^{40}Ar value less than three times the applied blank correction and is omitted. The next youngest crystal has a model age of 1.037 ± 0.088 Ma, which can be considered a maximum age for overlying sediments and archaeology, including the Acheulean site of Garba XIII.

MK27-19 This sample contains many xenocrysts and no clear juvenile population. The youngest crystal has an age of 1.429 ± 0.029 Ma, which can be considered a maximum age for overlying sediments and archaeology.

MK27-20 A weighted mean of individual crystals yields a single population with no apparent xenocrysts (Figure 6E, F). Step-heating of four multigrain aliquots a single plateau age of 0.797 ± 0.112 Ma (Figure 6G). An inverse isochron for these data yields an indistinguishable age (Figure 6H). The multigrain aliquots yield slightly older ages than the single crystal data. This could be

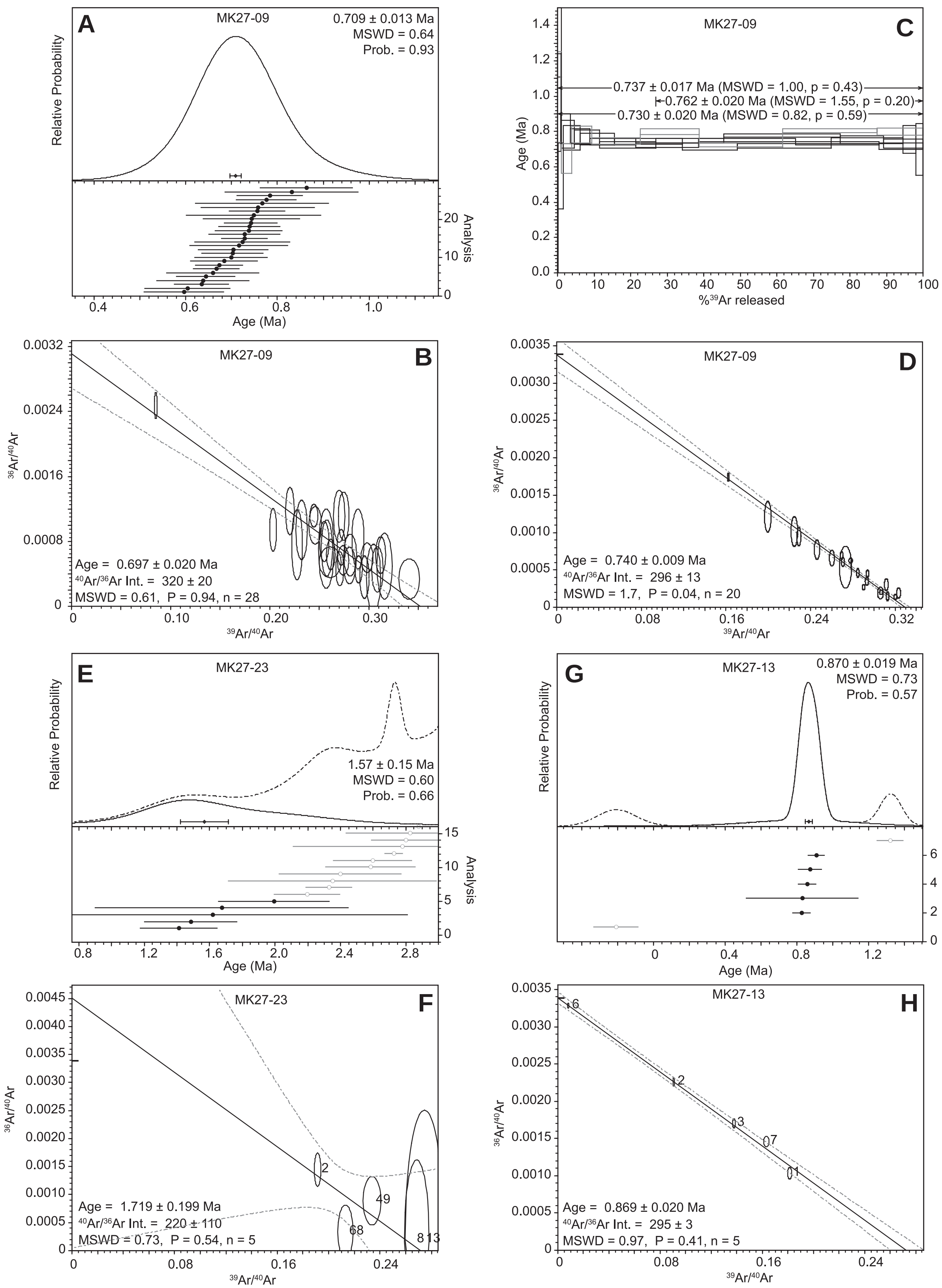

Figure 5. Age probability diagrams and inverse isochrons for single crystal total fusion data from (A, B) MK27-09, (E,F) MK27-23, (G, H) MK27-13, and age spectra and inverse isochrons (C, D) for incremental-heating data from MK27-09. Apparent xenocrysts are shown in gray in age probability diagrams and are not shown on isochrones. These are omitted from all age calculations. Incremental heating experiments not resulting in a plateau age are shown in gray in (C). Only analyses with sufficient ^{40}Ar (more than three times blank) are shown here. Isochrons (B, D, F, H) include only analyses from apparent juvenile populations. Only steps from plateaux containing more than 3% of the total ^{39}Ar released are shown on isochron from incremental heating data (D).

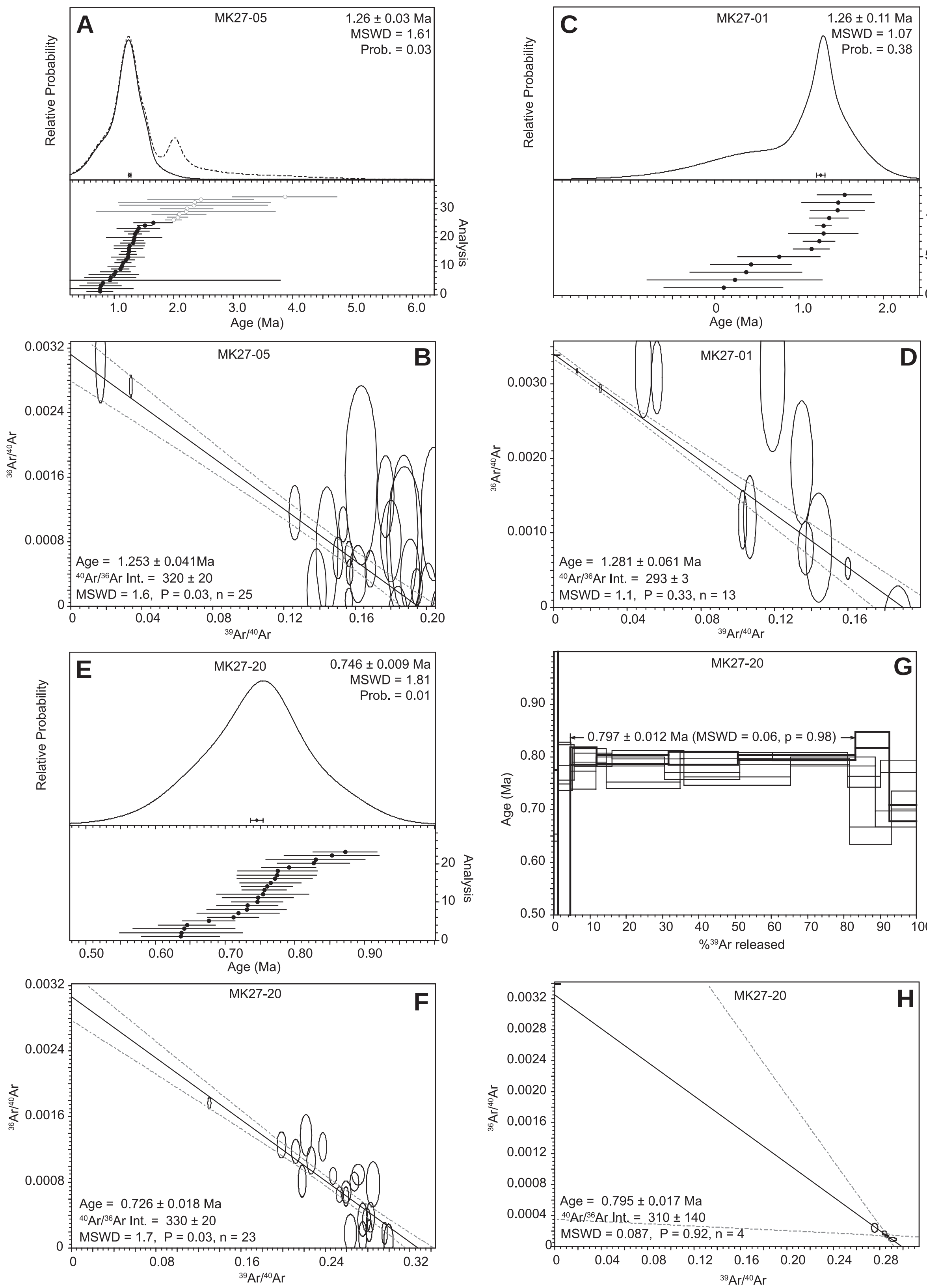

Figure 6. Age probability diagrams and inverse isochrons for single crystal total fusion data from (A, B) MK27-05, (C, D) MK27-01, (E, F) MK27-20, and inverse isochron and age spectra from (G, H) MK27-20. Apparent xenocrysts are shown in gray in age probability diagrams and are not shown on isochrones. These are omitted from all age calculations. The only incremental heating experiment to yield a plateau age is shown with thicker lines. Only analyses with sufficient ^{40}Ar (more than three times blank) are shown here. Isochrons (B, D, F) include only analyses from apparent juvenile populations. Steps from plateau containing less than 3% of the total ^{39}Ar released are shown in gray on the isochron from incremental heating data (H) and are not included in calculations.

explained by alteration more significantly manifest in the single grain total fusion data, but the possibility of xenocrystic contamination in the multigrained aliquots cannot be ruled out. The inverse isochron age for single crystal total fusion experiments (0.726 ± 0.018 Ma) is thus considered the most reliable age for this unit.

MK27-23 Multiple populations are present, but no conspicuous juvenile population exists. The first set of analyses, as reported in Morgan (2009), did yield an apparent juvenile population, but these runs are inferred to be affected by laboratory contamination (inadvertently loading grains from a different sample) and are thus not considered here. The presence of a sample of indistinguishable age (MK27-09) to the juvenile population in the same irradiation further supports this conclusion. Subsequent analyses (Figure 5E, F) show the presence of significant xenocrystic contamination and do not yield a consistent juvenile population. However, the youngest crystal with a reasonably well-constrained age (i.e., the uncertainty is <100% of the age) is dated to 1.414 ± 0.219 Ma. Furthermore, a group of the five youngest crystals yields a weighted mean age of 1.570 ± 0.150 Ma with an MSWD of 0.60 (Figure 5E), and an isochron age of 1.719 ± 0.199 Ma, with an MSWD of 0.73 (Figure 5F). Although these are clearly not ideally determined ages, they provide a reasonable maximum age for this and overlying units, and place useful constraints on paleomagnetic results, as discussed below. If the youngest grains are in fact juvenile, these ages can also place an important minimum age constraint on the obsidian artifacts found immediately underlying this unit.

Discussion

Reconciliation with magnetostratigraphy

The foregoing results allow us to place constraints on the ages of lithostratigraphic units, archaeology and magnetic reversals, which had previously been ‘hanging’ in time without a reliable absolute date to act as an anchor. Some discrepancies in various paleomagnetic studies have been clarified by new dates. However, difficulty in interpreting the stratigraphic sections that accompany some paleomagnetic studies prevents confident placement of all reversals onto the currently-used lithostratigraphic units. Refer to Figure 2(a, b, c).

At Gombore II (Figure 2b), we now have ages of 0.709 ± 0.013 Ma at the top of the Melka Kunture Formation, where sediments have been found to have normal polarity (Cressier, 1980; Tamrat, 1997), placing these sediments in the Brunhes Chron. Downsection, the polarity reverses (Cressier, 1980), and a tuff within the reverse interval is dated to 0.875 ± 0.010 Ma. Some discrepancy exists here with some paleomagnetic data (Tamrat, 1997) that indicated three reversals in that same section, which would place the lower tuff (MK27-08) in the period between the Jaramillo and Cobb Mountain subchrons by reference to the GPTS (Shackleton et al., 1990; Horng et al., 2002; Gradstein et al., 2004; Lourens et al., 2004). This is highly unlikely considering the $^{40}Ar/^{39}Ar$ data, and inspection of the paleomagnetic data shows the reversed interval was defined on only two samples (Tamrat, 1997) with opposing inclinations, thus the possibility of sample orientation error or that these reversed samples capture a short excursion within the Brunhes Chron cannot be excluded.

Further down the section in the Gombore I gully, the $^{40}Ar/^{39}Ar$ age constraints for sample MK27-12 have 2σ uncertainties too high to confidently place units into particular subchrons. However, there appear to be some sediments of normal polarity underlying sample MK27-12, which may have been deposited during either the Jaramillo or Cobb Mountain Subchron. Further downsection, there are parts of the section that seem to reliably indicate reversed polarity; this is in agreement with the age of sample MK27-03.

At Garba (Figure 2a), the top of the Melka Kunture Formation is similarly well constrained. An age of 0.869 ± 0.020 Ma for the uppermost tuff (MK27-13) is consistent with the reverse polarity found there, suggesting placement in the Matuyama Chron (Cressier, 1980). Again, the data become more difficult to interpret downsection, as the $^{40}Ar/^{39}Ar$ data did not reveal juvenile populations in samples MK27-16 and MK27-19. Since we only have maximum ages for these tuffs, assignment to a subchron cannot be made confidently. Additionally, the sample locations of previously published paleomagnetic studies are difficult to determine, further complicating interpretation. In one case, however, one study seems to capture a normal to reverse transition (Cressier, 1980), which may be the beginning of either the Jaramillo or Cobb Mountain Subchron. Although the age of the sample (MK27-16; <1.037 ± 0.088 Ma) should place this unit in the Jaramillo normal period, this age is within 1σ of Jaramillo time and within 2σ of Cobb Mountain time. Additionally, if the population with an inverse isochron age of 1.719 ± 0.199 Ma in MK27-23 is in fact a juvenile population, the apparently reversed polarity (Westphal et al., 1979; Cressier, 1980) would place it in the earliest portion of the Matuyama Chron, just above the Olduvai Subchron.

At Kella (Figure 2), the only paleomagnetic results are for the ignimbrite from the Kella Formation, which is found both there and at Melka Garba. Numerous paleomagnetic studies on this unit by Cressier (1980) clearly show a reversed polarity. This is in agreement with a $^{40}Ar/^{39}Ar$ age of 1.281 ± 0.061 Ma for the unit at Melka Garba and 1.253 ± 0.041 Ma at Kella, and places it in the reversed polarity subchron of the Matuyama following the Olduvai.

Paleoanthropological implications

These data allow more reliable age constraints to be placed on much of the stratigraphy, and thus archaeology and paleontology, at several localities within Melka Kunture.

Oldowan artifacts, including many made of obsidian, are likely from the Matuyama Chron, between the Jaramillo and Olduvai Subchrons, and thus between 1.072 and 1.778 Ma (Shackleton et al., 1990; Horng et al., 2002; Gradstein et al., 2004; Lourens et al., 2004). Less decisive $^{40}Ar/^{39}Ar$ geochronology suggests that some Oldowan obsidian artifacts are likely older than 1.393 ± 0.162 Ma (MK27-03) at Gombore I and possibly older than 1.719 ± 0.199 Ma (MK27-23) at Garba IV (Figure 2a, b). These dates also place constraints on the age of vertebrate fauna, including *Homo* specimens, from each of these localities.

Although less than ideal, results for sample MK27-23 suggest that the Oldowan obsidian artifacts found in levels E and F of the Garba IV excavation are the oldest known case of intensive (here >100 artifacts) exploitation of obsidian as a raw material for tool making. As noted in the introduction, the previously known earliest intensive use of obsidian is at Kariandusi, Kenya, which likely reaches back only to ∼1 Ma (Gowlett and Crompton, 1994). Other, less intensive use (generally <10 artifacts) possibly predates 1.48 Ma in the Acheulean at Gadeb locality 8E (Clark, 1979; Williams et al., 1979) but this is based on an unpublished K–Ar age on an alluvial unit, which are often plagued by xenocrystic contamination. As demonstrated in many studies (e.g., Morgan and Renne, 2008), K–Ar data from volcanic ashes with xenocrystic contamination are often shown to be unreliable by grain-specific $^{40}Ar/^{39}Ar$ work. Occasional obsidian artifacts are also found in several other localities, but they are exclusively in an Acheulean context and rarely, if ever, predate ∼1 Ma. Here, then, we may have increased the known time period of well-dated obsidian exploitation by ∼700 ka. As Piperno et al. (2009) discussed, it is unsurprising that the earliest use of obsidian would occur in such close proximity to the excellent source of obsidian at

Balchit. Whether earlier hominids eschewed obsidian or were simply unaware of it remains a question that may have fairly profound implications for the evolution of hominid cognitive skills; as obsidian gained increasing popularity in subsequent industries, its suitability for making specialized tools was increasingly recognized.

Additional age constraints can be assigned to the artifacts and vertebrate fauna found at Gombore II (Figure 2b), including the 'twisted bifaces' and *Homo* partial cranium from the Gombore II Locality 1 and the overlying possible butchery site at Locality 2. $^{40}Ar/^{39}Ar$ geochronology and some magnetostratigraphy (Westphal et al., 1979; Cressier, 1980) places them between 0.875 $\pm$ 0.010 Ma (MK27-08) and 0.709 $\pm$ 0.013 Ma (MK27-09). As these are the only known ages for twisted bifaces in Africa, the potential importance of these dates cannot yet be assessed.

At Gombore I, a tuff dated to 1.20 $\pm$ 0.07 Ma in the earliest portion of the Matuyama Chron, above the Olduvai Subchron, post-dates the Developed Oldowan from Gombore Iγ and constrains the beginning of the Acheulean at Melka Kunture. At Gabeb, on the east Main Ethiopian Rift border, the Developed Oldowan/early Acheulean sites recently revisited are dated to possibly >1.48 Ma and at least >0.7 Ma by the K–Ar method (Williams et al., 1979; Clark, 1979, 1987; de la Torre, 2011).

$^{40}Ar/^{39}Ar$ ages for Acheulean artifacts at Garba XIII (Figure 2a) are found between volcanic ashes with ages <1.037 $\pm$ 0.088 Ma and 0.869 $\pm$ 0.020 Ma, while archaeological horizons from Garba XII underlie a tuff dated to <0.772 $\pm$ 0.091 Ma. Early Acheulean artifacts at Simbiro III are older than 0.878 $\pm$ 0.014 Ma. At Kella III (Figure 2c), Oldowan artifacts are younger than 1.666 $\pm$ 0.009 Ma (Tables 1, 2). The large ignimbrite of the Kella Formation at Kella and Melka Garba is dated to 1.26 $\pm$ 0.07 Ma. This pre-dates classical Acheulean artifacts in the area. These dates form a unique record for the classical Acheulean of the high Ethiopian Plateau.

Conclusions

New $^{40}Ar/^{39}Ar$ data presented here allow, for the first time, significantly more precise age constraints to be placed upon the lithostratigraphy, archaeology and paleontology from Melka Kunture. Though some of the units could not be dated with the full current potential precision of the $^{40}Ar/^{39}Ar$ technique due to geologic complications, the new chronostratigraphy relieves dependence on previous magnetostratigraphic studies whose results are somewhat inconsistent.

This work helps constrain the timing of the tool manufacture using Oldowan, Acheulean, Middle Stone Age, and Late Stone Age technologies in this region. This allows for the first time a reliable and relatively complete timeline for the stratigraphic sequence, environmental changes, archaeology, and paleontology of this unique area. This contributes toward our understanding of the timing of human biological and behavioral evolution on the shoulder of the Ethiopian Rift.

Acknowledgements

We thank the Authority for Research and Conservation of the Cultural Heritage of Ethiopia, the Ministry of Culture and Tourism of Ethiopia, the Oromia Culture and Tourism Bureau, the Italian Archaeological Mission at Melka Kunture, and the National Museum of Ethiopia for permissions and facilitation. The Berkeley Geochronology Center $^{40}Ar/^{39}Ar$ geochronology lab was supported by the Ann and Gordon Getty Foundation and National Science Foundation grant BCS-0211172. Field work (L.M., G.K and J.P.R.) was partially funded by 'Région Aquitaine' grant 20071403002 for the 'Origines 1' project (J.P. Raynal director). We thank Jean Chavaillon, Giorgio Greco, Alain Queffelec, and the Melka Kunture excavation crew and staff for help in the field, and Abed Jaouni, Tim Becker, and Tim Teague for laboratory support. We thank an anonymous reviewer for a helpful review.

Appendix. Supplementary Data

Supplementary data related to this article can be found online at doi:10.1016/j.jhevol.2011.10.007.

References

Bailloud, G., 1965. Le gisement paléolithique de Melka-Kontouré. Institut Ethiopien d'Archéologie Cahier n 1, 1–37.
Bocherens, H., Koch, P.L., Mariotti, A., Geraads, D., Jaeger, J.J., 1996. Isotopic biogeochemistry (^{13}C, ^{18}O) of mammalian enamel from African Pleistocene hominid sites. Palaios 11, 306–318.
Cerling, T.E., Brown, F.H., Bowman, J.R., 1985. Low-temperature alteration of volcanic glass – Hydration, Na, K, O-18 and Ar mobility. Chem. Geol. 52, 281–293.
Chavaillon, J., 1979a. Stratigraphie du site archéologique de Melka-Kunturé (Ethiopie). Bull. Soc. Géol. Fr. 7, 227–232.
Chavaillon, J., 1979b. Un site acheuléen près du lac Langano, (Ethiopie). Abbay 10, 57–74.
Chavaillon, J., Berthelet, A., 2004. The archaeological sites of Melka Kunture. In: Chavaillon, J., Piperno, M. (Eds.), Studies on the Early Paleolithic Site of Melka Kunture, Ethiopia. Origines, Instituto Italiano di Preistoria e Protostoria, Firenze, pp. 25–80.
Chavaillon, J., Chavaillon, N., 1976. Le paléolithique ancien en Ethiopie, caractères techniques de l'Oldowayen de Gomboré I à Melka-Kunturé. Colloque V, IX° Congrés UISPP, Nice, pp. 43–69.
Chavaillon, J., Coppens, Y., 1975. Découverte d' Hominidé dans un site Acheuléen de Melka-Kunturé. Bulletins et Mémoires de la Société d'Anthropologie de Paris 2, 125–128.
Chavaillon, J., Coppens, Y., 1986. Nouvelle découverte d'*Homo erectus* à Melka-Kunturé. CR II 303 (1), 99–104.
Chavaillon, J., Piperno, M., 2004a. History of excavations at Melka Kunture. In: Chavaillon, J., Piperno, M. (Eds.), Studies on the Early Paleolithic Site of Melka Kunture, Ethiopia. Origines, Instituto Italiano di Preistoria e Protostoria, Firenze, pp. 3–23.
Chavaillon, J., Piperno, M. (Eds.), 2004b. Studies on the Early Paleolithic Site of Melka Kunture, Ethiopia. Origines, Istituto Italiano di Preistoria e Protostoria, Firenze.
Chavaillon, J., Brahimi, C., Coppens, Y., 1974. Première découverte d' Hominidé dans l'un des sites acheuléens de Melka-Kunturé (Ethiopie). CR Serie D 278, 3299–3302.
Chavaillon, J., Chavaillon, N., Coppens, Y., Senut, B., 1977. Présence d' Hominidé dans le site Oldowayen de Gomboré I à Melka-Kunturé. CR Serie D 285, 961–963.
Chavaillon, J., Hours, F., Coppens, Y., 1987. Découverte de restes humains fossiles associés à un outillage Acheuléen final à Melka-Kunturé (Ethiopie). CR II 304 (10), 539–542.
Clark, J.D., 1979. Hominid occupation of the east-central highlands of Ethiopia in the Plio-Pleistocene. Nature 282, 33–39.
Clark, J.D., 1987. Transitions: *Homo erectus* and the Acheulian: the Ethiopian sites of Gadeb and the Middle Awash. J. Hum. Evol. 16, 809–826.
Clark, J.D., Schick, K.D., 2000. Acheulean archaeology of the eastern Middle Awash. Annales Sciences Geologiques. In: de Heinzelin, J., Clark, J.D., Schick, K.D., Gilbert, W.H. (Eds.), The Acheulean and the Plio-Pleistocene Deposits of the Middle Awash Valley, Ethiopia. Royal Museum of Central Africa, Belgium, pp. 51–121.
Clark, J.D., Beyene, Y., WoldeGabriel, G., Hart, W.K., Renne, P.R., Gilbert, H., Defleur, A., Suwa, G., Katoh, S., Ludwig, K.R., Boisserie, J.R., Asfaw, B., White, T.D., 2003. Stratigraphic, chronological and behavioural contexts of Pleistocene *Homo sapiens* from Middle Awash, Ethiopia. Nature 423, 747–752.
Condemi, S., 2004. The Garba IV E mandible. In: Chavaillon, J., Piperno, M. (Eds.), Studies on the Early Paleolithic Site of Melka Kunture, Ethiopia. Origines, Instituto Italiano di Preistoria e Protostoria, Firenze, pp. 687–701.
Coppens, Y., 2004. The hominids of Melka Kunture. Some general reflections. In: Chavaillon, J., Piperno, M. (Eds.), Studies on the Early Paleolithic Site of Melka Kunture, Ethiopia. Origines, Instituto Italiano di Preistoria e Protostoria, Firenze, pp. 685–686.
Cressier, P., 1980. Magnétostratigraphiedu gisement Pléistocène de Melka-Kunturé (Ethiopie). Datation des niveaux oldowayens et acheuléens. Ph.D. Dissertation, L'Université Louis Pasteur.
Crompton, R.H., Gowlett, J.A.J., 1993. Allometry and multidimensional form in Acheulean bifaces from Kilombe, Kenya. J. Hum. Evol. 25, 175–199.
de la Torre, I., 2011. The early Stone age lithic assemblages of Gadeb (Ethiopia) and the Developed Oldowan/early Acheulean in east Africa. J. Hum. Evol. 60, 768–812.
Deino, A.L., Potts, R., 1990. Single-Crystal $^{40}Ar/^{39}Ar$ dating of the Olorgesailie Formation, Southern Kenya rift. J. Geophys. Res. 95, 8453–8470.

Gallotti, R., Collina, C., Raynal, J.-P., Kieffer, G., Geraads, D., Piperno, M., 2010. The early Middle Pleistocene site of Gombore II (Melka Kunture, Upper Awash, Ethiopia) and the issue of Acheulean bifacial shaping strategies. Afr. Archaeol. Rev. 27, 291–322.

Geraads, D., 1979. La faune des gisements de Melka Kunturé (Ethiopie): Artiodactyles, Primates. Abbay 10, 21–49.

Geraads, D., Eisenmann, V., Petter, G., 2004. The large mammal fauna of the Oldowan sites of Melka Kunture. In: Chavaillon, J., Piperno, M. (Eds.), Studies on the Early Paleolithic Site of Melka Kunture, Ethiopia. Origines, Istituto Italiano di Preistoria e Protostoria, Firenze, pp. 169–192.

Gowlett, J.A.J., 1993. Le site Acheuléen de Kilombe: stratigraphie, géochronologie, habitat et industrie lithique. L'Anthropologie 97, 69–84.

Gowlett, J.A.J., Crompton, R.H., 1994. Kariandusi: Acheulean morphology and the question of allometry. Afr. Archaeol. Rev. 12, 3–42.

Gradstein, F.M., Ogg, J.G., Smith, A.G. (Eds.), 2004. A Geologic Time Scale 2004. Cambridge University Press.

Hay, R.L., 1976. Geology of the Olduvai Gorge: a Study of Sedimentation in a Semiarid Basin. University of California Press, Berkeley and Los Angeles, California.

Horng, C.-S., Lee, M.-Y., Palike, H., Wei, K.-Y., Liang, W.-T., Iizuka, Y., Torii, M., 2002. Astronomically calibrated ages for geomagnetic reversals within the Matuyama chron. Earth Planets Space 54 (6), 679–690.

Isaac, G.L., 1977. Olorgesailie: Archaeological Studies of a Middle Pleistocene Lake Basin in Kenya. University of Chicago Press.

Leakey, L.S.B., 1931. The Stone Age Cultures of Kenya Colony. The University Press, Cambridge, England.

Lee, J.-Y., Marti, K., Severinghaus, J.P., Kawamura, K., Yoo, H.-S., Lee, J.B., Kim, J.S., 2006. A redetermination of the isotopic abundances of atmospheric Ar. Geochimica et Cosmochimica Acta 70, 4507–4512.

Lourens, L., Hilgen, F., Shackleton, N.J., Laskar, J., Wilson, J., 2004. Orbital tuning calibrations and conversions for the Neogene Period. Appendix 2. In: Gradstein, F.M., Ogg, J.G., Smith, A.G. (Eds.), A Geologic Time Scale 2004. Cambridge University Press, pp. 467–471.

Merrick, H.V., Brown, F.H., 1984. Obsidian sources and patterns of source utilization in Kenya and northern Tanzania: some initial findings. Afr. Archaeol. Rev. 2, 129–152.

Montgelard, C., Catzeflis, F.M., Douzery, E., 1997. Phylogenetic relationships of artiodactyls and cetaceans as deduced from the comparison of cytochrome b and 12S rRNA mitochrondrial sequences. Mol. Biol. Evol. 14, 550–559.

Morgan, L.E., 2009. Geochronological constraints on Plio-Pleistocene hominid evolution in the Ethiopian rift. Ph.D. Dissertation, University of California, Berkeley.

Morgan, L.E., Renne, P.R., 2008. Diachronous dawn of Africa's Middle Stone age: new $^{40}Ar/^{39}Ar$ ages from the Ethiopian rift. Geology 36, 967–970.

Morgan, L.E., Renne, P.R., Taylor, R.E., WoldeGabriel, G., 2009. Archaeological age constraints from extrusion ages of obsidian: examples from the Middle Awash, Ethiopia. Quatern. Geochronol. 4, 193–203.

Negash, A., Shackley, M.S., Alene, M., 2006. Source provenance of obsidian artifacts from the early Stone age (ESA) site of Melka Konture, Ethiopia. J. Archaeol. Sci. 33, 1647–1650.

Nomade, S., Renne, P.R., Vogel, N., Deino, A.L., Sharp, W.D., Becker, T.A., Jaouni, A.R., Mundil, R., 2005. Alder Creek sanidine (ACs-2): a Quaternary Ar-40/Ar-39 dating standard tied to the Cobb Mountain geomagnetic event. Chem. Geology. 218, 315–338.

Piperno, M., Collina, C., Gallotti, R., Raynal, J.-P., Kieffer, G., Bourdonnec, F.X.L., Poupeau, G., Geraads, D., 2009. Obsidian exploitation and utilization during the Oldowan at Melka Kunture (Ethiopia). In: Hovers, E., Braun, D.R. (Eds.), Interdisciplinary Approaches to the Oldowan. Springer, Dordrecht, pp. 111–128.

Poupeau, G., Kieffer, G., Raynal, J.-P., Milton, A., Delerue, S., 2004. Trace element geochemistry in Balchit obsidian (Upper Awash, Ethiopia). In: Chavaillon, J., Piperno, M. (Eds.), Studies on the Early Paleolithic Site of Melka Kunture, Ethiopia. Origines, Instituto Italiano di Preistoria e Protostoria, Firenze, pp. 103–110.

Raynal, J.-P., Kieffer, G., 2004. Lithology, dynamism and volcanic successions at Melka Kunture (Upper Awash, Ethiopia). In: Chavaillon, J., Piperno, M. (Eds.), Studies on the Early Paleolithic Site of Melka Kunture, Ethiopia. Origines, Istituto Italiano di Preistoria e Protostoria, Firenze, pp. 111–135.

Raynal, J.-P., Kieffer, G., Bardin, G., 2004. Garba IV and the Melka Kunture Formation. A preliminary lithostratigraphic approach. In: Chavaillon, J., Piperno, M. (Eds.), Studies on the Early Paleolithic Site of Melka Kunture, Ethiopia. Origines, Istituto Italiano di Preistoria e Protostoria, Firenze, pp. 137–166.

Renne, P.R., Norman, E.B., 2001. Determination of the half-life of 37Ar by mass spectrometry. Physiol. Rev. C 63, n.p.

Renne, P.R., Knight, K.B., Nomade, S., Leung, K.N., Lou, T.P., 2005. Application of deuteron-deuteron (D-D) fusion neutrons to Ar-40/Ar-39 geochronology. Appl. Radiat. Isot. 62, 25–32.

Renne, P.R., Cassata, W.S., Morgan, L.E., 2009. The isotopic composition of atmospheric argon and 40Ar/39Ar geochronology: time for a change? Quatern. Geochronol. 4, 288–298.

Renne, P.R., Mundil, R., Balco, G., Min, K., Ludwig, K.R., 2010. Joint determination of 40K decay constants and 40Ar*/40K for the Fish Canyon sanidine standard, and improved accuracy for 40Ar/39Ar geochronology. Geochimica et Cosmochimica Acta 74, 5349–5367.

SAS Institute, Inc., 2007. JMP® Software. Cary, NC.

Schmitt, J.-J., Wempler, J.-M., Chavaillon, J., Andrews, M.C., 1977. Initial K-Ar and paleomagnetic results of the Melka Kunture early-man sites, Ethiopia. In: Proceedings VIII Panafrican Congress of Prehistory and Quaternary studies, Nairobi.

Shackleton, N.J., Berger, A., Peltier, W.R., 1990. An alternative astronomical calibration of the lower Pleistocene timescale based on ODP site 677. Trans. R. Soc. Edinburgh-Earth Sci. 81, 251–261.

Steiger, R.H., Jäger, E., 1977. Subcommission on geochronology: convention on the use of decay constants in geo- and cosmochemistry. Earth Planet. Sci. Lett. 36, 359–362.

Taieb, M., 1974. Evolution quaternaire du bassin de l'Awash (Rift Ethiopien et Afar). Ph.D. Dissertation, Université Paris IV.

Tamrat, E., 1997. Magnétostratigraphie et magnétisme de séquences lacustres Plio-Pléistocène et Holocène d'Afrique Orientale. Ph.D. Dissertation, University d'Aix-Marseille III.

Valkiers, S., Vendelbo, D., Berglund, M., de Podesta, M., 2010. Preparation of argon Primary Measurement Standards for the calibration of ion current ratios measured in argon. Int. J. Mass Spectrom. 291, 41–47.

Walter, D., 1996. Twisted Bifaces: an Analysis of Intentionality and Functional Efficiency of Twisted Bifaces in the British Paleolithic. Ph.D. Dissertation, University of London.

Westphal, M., Chavaillon, J., Jaeger, J.J., 1979. Magnétostratigraphie des dépôts Pléistocènes de Melka-Kunturé (Ethiopie): premières données. Bull. Soc. Géol. Fr. 7, 237–241.

White, M.J., 1998. Twisted Ovate bifaces in the British lower Palaeolithic: some Observations and implications. Lithic Studies Society Occasional Paper 6. In: Ashton, N., Healy, F., Pettitt, P. (Eds.), Stone Age Archaeology: Essays in Honour of John Wymer. Oxbow Books, pp. 98–104.

Williams, M.A.J., Williams, F.M., Gasse, F., Curtis, G.H., Adamson, D.A., 1979. Plio-Pleistocene environments at Gadeb prehistoric site, Ethiopia. Nature 282, 29–33.

Zilberman, U., Smith, P., Piperno, M., Condemi, S., 2004a. Evidence of amelogenesis imperfecta in an early African *Homo erectus*. J. Hum. Evol. 46 (6), 647–655.

Zilberman, U., Smith, P., Condemi, S., 2004b. Evidence for a genetic disorder affecting tooth formation in the Garba IV child. In: Chavaillon, J., Piperno, M. (Eds.), Studies on the Early Paleolithic Site of Melka Kunture, Ethiopia. Origines, Istituto Italiano di Preistoria e Protostoria, Firenze, pp. 703–713.